ISSN 1075-7015, Geology of Ore Deposits, 2019, Vol. 61, No. 8, pp. 827–842. © Pleiades Publishing, Ltd., 2019.
Russian Text © The Author(s), 2019, published in Zapiski Rossiiskogo Mineralogicheskogo Obshchestva, 2019, No. 1, pp. 79–99.

MINERALS AND MINERAL PARAGENESES

New Data on Epidote-Supergroup Minerals: Unusual Chemical Compositions, Typochemistry, and Raman Spectroscopy

D. A. Varlamov[a, b, *], V. N. Ermolaeva[b, c, **], N. V. Chukanov[a, d, *], S. Jančev[e], M. F. Vigasina[d], and P. Yu. Plechov[d, f]**

[a] *Institute of Problems of Chemical Physics, Russian Academy of Sciences, Chernogolovka, 142432 Russia*
[b] *Korzhinskii Institute of Experimental Mineralogy, Russian Academy of Sciences, Chernogolovka, 142432 Russia*
[c] *Vernadsky Institute of Geochemistry and Analytical Chemistry, Russian Academy of Sciences, Moscow, 119991 Russia*
[d] *Faculty of Geology, Moscow State University, Moscow, 119991 Russia*
[e] *Faculty of Technology and Metallurgy, Saints Cyril and Methodius University, Skopje, Macedonia*
[f] *Fersman Mineralogical Museum, Russian Academy of Sciences, Moscow, 119071 Russia*
**e-mail: dima@iem.ac.ru*
***e-mail: cvera@mail.ru*
****e-mail: chukanov@icp.ac.ru*

Received October 15, 2018; revised October 26, 2018; accepted October 26, 2018

Abstract—Compositional variations of the epidote-supergroup minerals from the different magmatic, metasomatic, and metamorphic formations of the Pelagonian Massif (Republic of North Macedonia), the Urals (Russia) and the Eifel Mountains (Germany) were studied. The new data on isomorphism in these minerals were obtained. Nine potentially new mineral species belonging to the epidote supergroup including the minerals, in which Cr, Ga, La, Ce, Nd, and Pb are the species-defining components, as well as a number of varieties with unusually high Zn and Cu contents, were identified. The relationship between the chemical composition of epidote-supergroup minerals and their Raman spectra is discussed.

Keywords: minerals of the epidote supergroup, typomorphism, Raman spectra, Pelagonian massif, Republic of Macedonia

DOI: 10.1134/S1075701519080130

INTRODUCTION

The epidote supergroup minerals (ESM) include monoclinic ortho–diorthosilicates with a general formulae $A1A2M1M2M3(Si_2O_7)(SiO_4)Ø4Ø10$, where $A1$ = Ca, Mn^{2+}; $A2$ = **Ca**, ***REE***, **Sr**, **Pb**, Th; $M1$ = **Al**, **Fe^{3+}**, **V^{3+}**, **Mn^{3+}**, Cr^{3+}; $M2$ = **Al**, Fe^{3+}; $M3$ = **Al**, **Fe^{3+}**, V^{3+}, **Mn^{3+}**, Cr^{3+}, **Mg**, **Fe^{2+}**, **Mn^{2+}**; $Ø4$ = O, F; $Ø10$ = O, OH (the components playing the species-forming role in the known ESMs are indicated in bold). Based on the charges of cations and anions dominating in the different sites of the crystal structure, four mineral groups are distinguished within the epidote supergroup (Armbruster et al., 2006; Mills et al., 2009; Chukanov et al., 2010). They correspond to the following general formulae:

the epidote group, $A1^{2+}A2^{2+}M1^{3+}M2^{3+}M3^{3+}(Si_2O_7)(SiO_4)O(OH)$;

the allanite group, $A1^{2+}A2^{3+}M1^{3+}M2^{3+}M3^{2+}(Si_2O_7)(SiO_4)O(OH)$;

the dollaseite group, $A1^{2+}A2^{3+}M1^{2+}M2^{3+}M3^{2+}(Si_2O_7)(SiO_4)F(OH)$;

the askagenite group, $A1^{2+}A2^{3+}M1^{3+}M2^{3+}M3^{3+}(Si_2O_7)(SiO_4)O_2$.

The ESMs are characterized by a wide isomorphism in all cationic positions, except for the octahedral site $M2$, which is predominantly occupied by Al (often with minor Fe^{3+}) in all studied samples. The heterovalent isomorphism in the $M1$ site is accompanied by O ↔ F substitutions in the $Ø4$ site, while the $Ø10$ site demonstrates clear affinity to the OH group due to the strong hydrogen bond, which results in stabilization of the crystal structure.

From a practical point, the most interesting are the REE members of the epidote supergroup, mostly as the components of REE ores, as well as probable prototypes of synthetic materials applicable as the components of immobilizing matrixes for actinides and ^{90}Sr. In addition, with account for a wide abundance of ESMs in different geological formations and vari-

ability in their chemical composition, we may consider the crystallochemical patterns of these minerals as an important typomorphic indicator of the mineral-forming conditions, mostly the medium chemistry. Here we report the data on the chemical composition that significantly expand our knowledge of the chemical variations in the ESMs and Raman spectroscopy of these silicates.

METHODS OF THE STUDY

The composition of the samples was studied by the method of X-ray spectral microanalysis on a Tescan Vega-II XMU scanning electron microscope and an INCA Energy 450 system of registration of X-ray radiation and calculation of the sample composition (the EDS mode with an accelerating voltage of 20 kV and an electron beam current of 400 nA). The period of signal accumulation was 100 s. The diameter of an excitation zone did not exceed 5 μm. During the electron microprobe analyses, the electron beam diameter was within 157–180 nm. The images were obtained with magnifications from 302× to 1670× in a scanning mode, at an electron beam diameter of 60 nm. The more detailed description of the method was given in (Ermolaeva et al., 2016; Varlamov et al., 2017).

The Raman spectra of randomly oriented Samples 4, 14, and 15 were obtained in a frequency range from 100 to 1200 cm^{-1} on an XPloRA automatic Raman spectrometer (Horiba Scientific) equipped with a multichannel detector combined with a confocal microscope including the connecting and filtering optics. The focal distance of a spectrometer is 200 mm. We used laser radiation with a wavelength of 532 nm and a nominal power of 25 mW. To decrease the influence of luminescence, some spectra were taken several times in one spot. The study was carried out using a spectral cell 2400T (2400 hatches per mm). The period of accumulation of each spectrum window was 90 s (three times by 30 s) in the mode of automatic combination of windows with overlapping by 100 lines. The initial spectra processing was performed using the LabSpec v. 5.78.24 software.

The Raman spectra of other samples were obtained on an EnSpectr R532-20 Raman microscope (Russia) in a frequency range from 100 to 4000 cm^{-1} with a resolution of 6 cm^{-1}. The wavelength of exciting radiation of a diode laser was 532 nm; a radiation output power was 15–20 mW. The dispersion of scattered radiation was carried out by a holographic diffraction grating with 1800 hatches per mm. The spectra were obtained with a magnification of 40×, exposure of 1 or 2 s, and averaging by 100, 50, and 30 exposures, respectively. The diameter of a focal spot of laser radiation was ~10 μm.

DESCRIPTION OF THE ESM SAMPLES STUDIED AND A BRIEF CHARACTERISTIC OF THE OBJECTS, FROM WHICH THEY ARE FORMED

Samples of the ESMs from the different mineral associations of the metasomatic, pneumatolytic, and regional metamorphic origin and characterized by wide variations in the chemical composition are the objects of this study.

Samples 1–7 were collected in ore occurrences from the Pelagonian Massif, in the region of the Nežilov Village (Republic of North Macedonia). In this area, the metasomatic rocks with the high concentrations of chalcophile elements (S, As, Sb, Zn, Pb, and Cu) compose an endocontact zone between metarhyolite, aporhyolite schist and dolomite marble and baryte schist (Barić, 1960). A characteristic feature of these rocks is that, in contrast to most of polymetallic ores of the endogenic origin, they almost do not contain sulfides and sulfosalts, while the chalcophile elements enter the composition of oxygen-bearing compounds, mostly oxides, silicates, phosphates, and arsenates. The mineral parageneses of ore-bearing metasomatic rocks of the Nežilov area were previously described in (Chukanov et al., 2015, 2016, 2018; Ermolaeva et al., 2016, 2018; Jančev et al., 2016; Varlamov et al., 2017a). It is assumed that the absence of sulfides in these associations, results from the high activity of barium, as well as from the oxidizing environment of the ore formation.

ESMs from the ore occurrences of the Pelagonian Massif form anhedral ore rarely subhedral grains with sizes up to a few cm (usually not larger than 1 mm), sometimes with the complex inner zoning. They form polymineral aggregates, mostly composed of baryte or tilasite, with low contents of dolomite and quartz. In these aggregates, ESMs closely associate with the minerals of the högbomite supergroup, Zn-bearing members of the spinel group, hematite, albite, potassic feldspar, quartz, dolomite, calcite, hematite, Zn-bearing clinopyroxenes, amphiboles, phlogopite, chlorite, and talc. Among the accessory minerals in these associations are Sb^{5+}- and Ti-dominant minerals of the pyrochlore supergroup, zircon, As-bearing apatite, hydroxyl-bearing hedyphane, almeidaite, nežilovite, tripuhyite, mottramite, and different manganese oxides. Some samples are characterized by the high concentrations of Cu (up to ~0.1 pfu in Samples 1, 6, and 7) and Zn (up to ~0.2–0.3 pfu in Samples 1, 6, and 7).

In **Sample 1** (Fig. 1a) mostly composed of an aggregate of baryte and magnesioriebeckite, ESMs form individuals of two types: small (~10 μm) not containing REEs and larger ones (~100 μm). The central and peripheral zones of the latter type, mostly represented by piemontite, contain up to 0.2–0.4 pfu REEs and 0.13–0.85 pfu Pb.

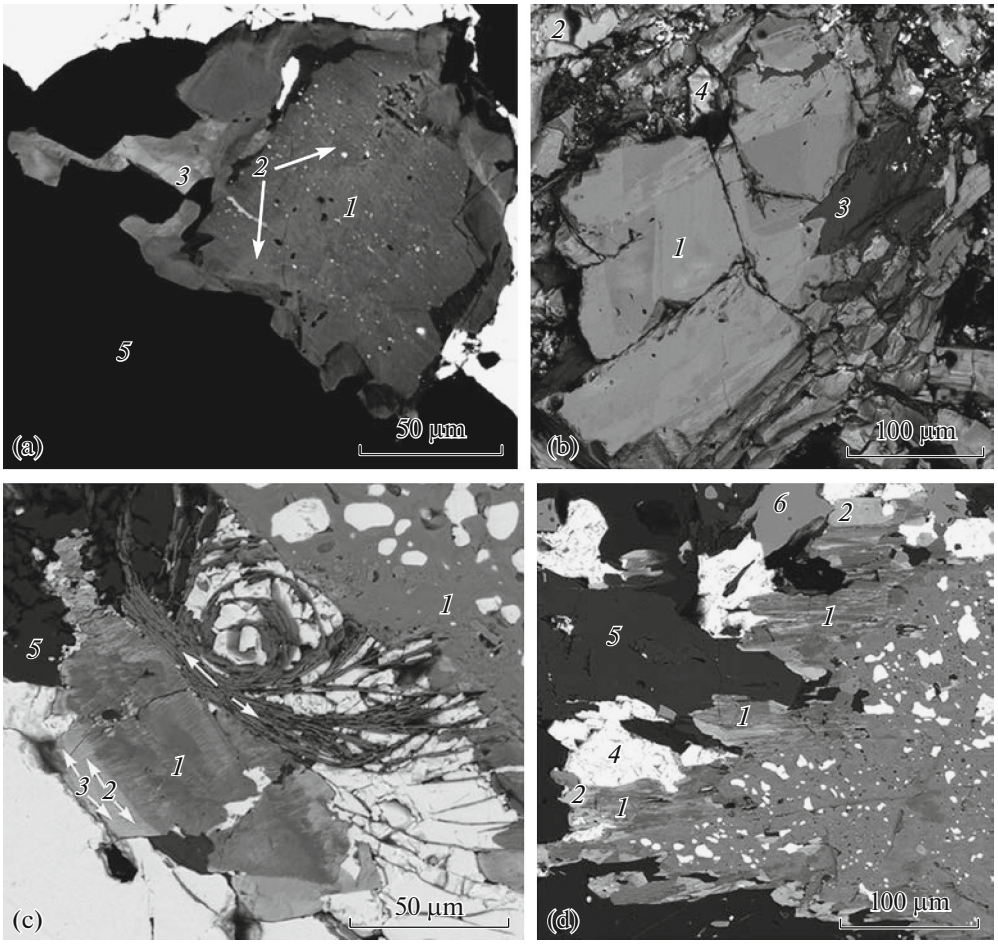

Fig. 1. BSE images of polished sections. (a) Grain of epidote-supergroup minerals with zones of piemontite (*1*), allanite-(Ce) (*2*), "ferripiemontite-(Pb)" (*3*) in association with baryte (*4*) and magnesioriebeckite (*5*) (Sample 1); (b) piemontite (*1*) with zones containing up to 3–4 wt % PbO (light areas) in granular aggregate of tilasite (*2*), in association with quartz (*3*) and baryte (*4*) (Sample 2); (c) piemontite grains (*1*) with outer zones of piemontite-(Pb) (*2*) and "ferripiemontite-(Pb)" (*3*) in baryte (*4*), in association with albite (*5*) and zincohögbomite (*6*) (Sample 6); (d) fragment of zoned piemontite–piemontite-(Pb) (*1*) with areas of "ferripiemontite-(Pb)" (*2*) in association with quartz (*3*), baryte (*4*), magnesioriebeckite (*5*), and hematite (*6*) (Sample 6).

In **Sample 2** (Fig. 1b), zoned grains of piemontite (with a Pb content from 0.03 to 0.17 pfu and a size of 0.2–0.3 mm) and their aggregates associate with baryte and tilasite and almost do not contain REEs.

In **Sample 3**, piemontite and piemontite-(Pb) form small (~10 μm) segregations in association with aegirine-augite, magnesioriebeckite, ferribarroisite, albite, tilasite, hydroxycalciоromeite, and fluorcalciоromeite. These ESMs almost do not contain REEs as well.

Samples 4a and 4b are the fragments of a piemontite-(Pb) holotype previously described by Chukanov et al. (2012). In addition to the prismatic crystals of piemontite-(Pb) with the composition $Ca(Pb_{0.73}Ca_{0.30})(Al_{0.65}Fe^{3+}_{0.34})Al(Mn^{3+}_{0.67}Fe^{3+}_{0.33})(Si_{2.96}Al_{0.04})O_{12}(OH)$ and a length up to 1 mm subjected to tectonic crushing, there are small (up to 20 μm) anhedral (sometimes round) grains of piemontite-(Pb) and La-dominant ESM containing 0.3–0.5 pfu REE. Among the major minerals of these samples are cellular zoned baryte, talc, and clinopyroxene.

In **Sample 5**, piemontite, "ferripiemontite", and epidote containing up to 0.27 pfu Pb form small (~5 μm) almost REE-free inclusions in hydroxyplumboromeite and small (~5 μm) grains of irregular shape in calcite, in association with hematite, quartz, tilasite, and minerals of the pyrochlore supergroup (hydroxycalciоromeite, fluorocalciоromeite, and hydroxyplumboromeite) containing up to 0.2 pfu REEs.

ESMs in **Sample 6** form zoned (with the zones of piemontite, piemontite-(Pb), "ferripiemontite-Pb" and epidote) individuals with a size up to 1 mm, sometimes with the areas enriched in REEs (up to 0.4 pfu), as well as small (~10 μm) grains almost REE-free, in association with baryte, albite, quartz, gahnite, franklinite, zincohögbomite, zincovelesite, and

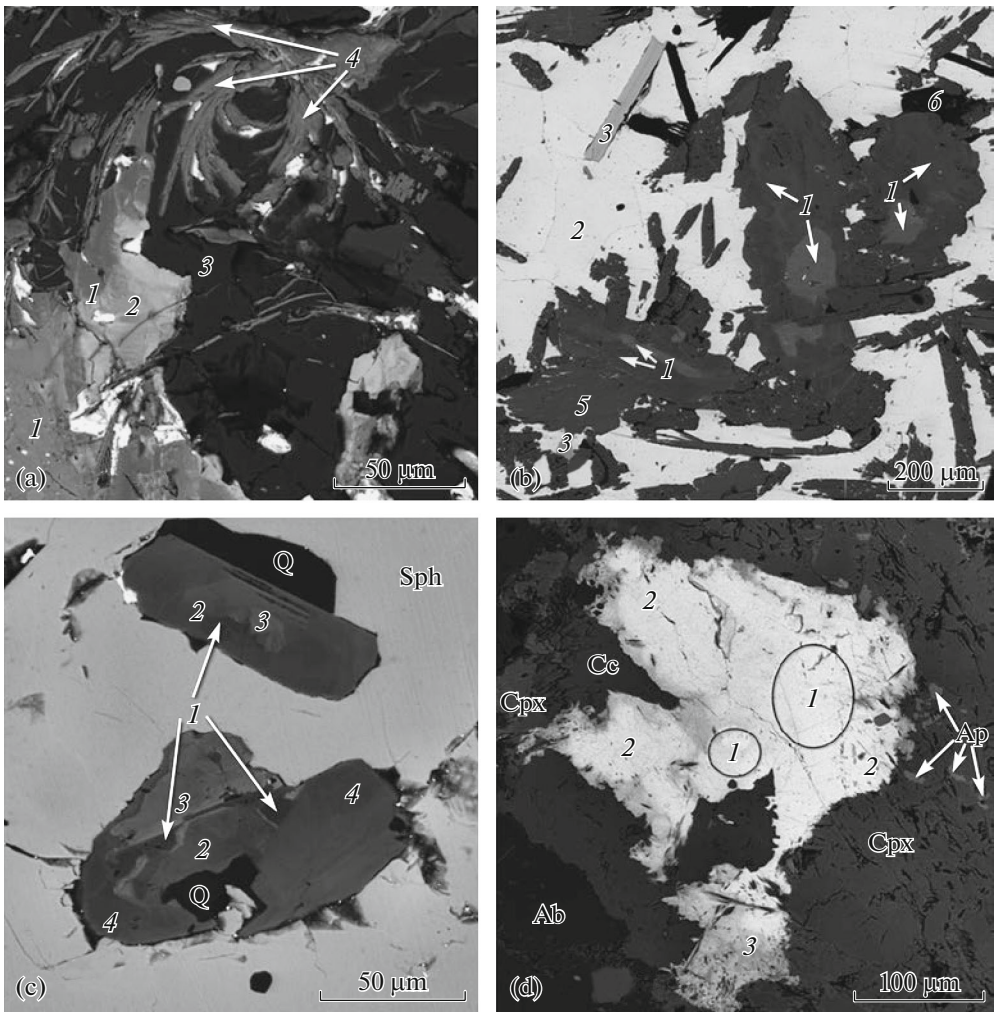

Fig. 2. BSE images of polished sections. (a) Individual of epidote-supergroup minerals with piemontite (*1*) and piemontite-(Pb) (*2*) zones in association with magnesioriebeckite (*3*) and Mn^{4+}-analogue of zincohögbomite (*4*) (Sample 6); (b) zoned individuals of epidote (*1*) in baryte aggregate (*2*), in association with nežilovite (*3*), almeidaite (*4*), zincohögbomite (*5*), and Zn-bearing talc (6) (Sample 7); (c) grains of epidote-supergroup minerals in sphalerite with zones of Ga analogue of epidote (*1*), Ga-rich allanite *2*), low-Ga allanite (*3*), and epidote (*4*) (Sample 4); (d) grain of epidote-supergroup minerals with zones of Cr-dominant allanite-group mineral (*1*, see analyses 9 and 10 in Table 2), allanite-(Ce) (*2*), and epidote (*3*) (Sample 15).

hydroxyplumboromeite. Large ESM grains contain abundant inclusions of baryte and zincohögbomite (Figs. 1c, 1d, and 2a).

In **Sample 7** (Fig. 2b), large (0.5–1 mm) segregations of epidote with a Pb content from 0.11 to 0.48 pfu occur in barite and associate with Zn-bearing talc, zincohögbomite, gahnite, tripuhyite, almeidaite, and nežilovite. Epidote is zoned, the central parts of grains are enriched in REEs (0.14–0.36 pfu), Zn (0.18–0.36 pfu), and Cu (0.05–0.09 pfu), while the outer zones almost do not contain REEs (0.04–0.06 pfu), Zn (0–0.07 pfu), and Cu (0.02–0.04 pfu).

Sample 8 was collected from the complex of aporhyolitic schist outcropped in the area of Lake Grubependity, in the zone of an interformational contact (IFC) between the Precambrian tectonic complex of Preuralides and the Paleozoic complex of Uralides on the Maldynyrd Ridge (Subpolar Urals). This formation was described in detail by Yudovich et al. (2001). At least two tectonic zones of various ages are observed within the Maldinskii Fault. These zones are composed of micaceous–chloritoid schist, aporhyolitic pyrophyllite schist, conglomerate, diabase, and intruding rhyolite with the polymetallic mineralization at the contacts. Greisenized aporhyolitic formations are characterized by the high REE concentrations. Microprobe studies of the mineral forms of REEs showed the presence of phosphates, arsenates, silicates, molibdates–wolframates, many of which are most likely the new minerals. The major minerals accumulating REEs in aporhyolitic schist are phosphates and arsenates; among silicates, are the allanite-group minerals. Exotic accessory phases include REE arsenates (Yudovich et al., 2001).

The complex of aporhyolitic schist from the area of Lake Grubependity contain widely abundant concretions composed of the spessartine–epidote–quartz aggregates, geochemically characterized by the anomalously high concentration of Mn (up to 3.4 wt % MnO, on the average, 2.72%) and As (up to 1%), as well as by the high REE concentrations (on the average, ten times higher than those in rhyolite). As was reported by Yudovich with co-workers (2001), there are individual crystals and aggregates of Mn-and REE-bearing ESMs of at least two generations. Sample 8 is a fragment of such segregation formed by a fine-granular aggregate, mostly composed of quartz, spessartine, and muscovite, as well as accessory xenotime-(Y), chernovite-(Y), gasparite-(Nd), ardennite, and different minerals of the epidote supergroup. These minerals form anhedral grains with a size not exceeding 20 μm.

Samples 9 and 10 are represented by eruptive fragments of nosean sanidinite collected in the In den Dellen Mine near the Laacher See (Eifel Mountains, Rheinland-Pfalz, Germany), which is a caldera of paleovolcano. The origin of these rocks has been discussed in detail in some publications (Frechen, 1947; Schmitt, 2006; Schmitt et al., 2010; Chukanov et al., 2014). Nosean syenite from the Laacher Volcano is interpreted as a rock comagmatic to nosean–cancrinite–nepheline syenite and host phonolite. Crystallization of nosean syenite occurred in the upper part of magmatic chamber at a temperature below 700°C, 5000–20000 years prior to the last eruption, which occurred 12900 years ago. This rock is characterized by the presence of various accessory minerals of rare elements (Nb, Zr, REE, U, and Th), most likely of the pneumatolytic origin, which crystallized on walls of cavities in sanidinite. Due to the young geological age of rocks of the Laacher Volcano, the minerals with impurities of radioactive elements are not metamict and have complete crystal structures. Sample 10 contains ferriakasakaite-(La) and was previously describe in detail by Chukanov et al. (2018).

Sample 11 is from the Mochalin Lug rare-earth occurrence, in the exocontact zone of the Potaniny Mt alkaline intrusion (South Urals), and is an ovoid with a size of 2 × 4 cm, mostly composed of ferriallanite-(La), bastnaesite-(La), bastnaesite-(Ce), toernebohmite-(La), fluorbritholite-(La), and minerals of the gatelite group. The formation of rare-earth minerals there most likely results from the process of fenitization of granite pegmatite. The detailed characterization of mineralogy of the Mochalin Log deposit was given by Zil'bermints (1930), Kuznetsov (1930), Svyazhin (1956), and Pekov with co-workers (2002). Ferriallanite-(La) in Sample 11 forms monomineral fine-granular aggregates of the black color with a size up to 5 × 7 mm and intergrowths with poorly studied La mineral of the gatelite group.

Sample 12 is represented by isometric piemontite crystals of the dark red color with a size up to 5 mm associated with spessartine and svabite, which is from the Rakten Mn ore occurrence (Jokkmokk, North Sweden) related to the low-grade metamorphic formation (Ödman, 1950). The empirical formula of this piemontite is $(Ca_{1.96}Na_{0.06})_{\Sigma 1.02}(Al_{0.78}Fe^{3+}_{0.21}Ti_{0.01})_{\Sigma 1.00}Al(Mn^{3+}_{0.68}Fe^{3+}_{0.32})_{\Sigma 1.00}Si_3O_{12}(OH)$.

Sample 13 is from the Trimouns talc deposit occurring near the Luzenac Village in the French Pyrenees. It is represented by black prismatic crystals of dissakisite-(Ce) with a length up to 5 mm from the association with talc and dolomite. The Trimouns deposit has a metasomatic origin and is described in detail by Moine et al. (1989) and Piret et al. (1990). The empirical formula of ESM from Sample 13 is $(Ca_{0.93}Na_{0.07})_{\Sigma 1.00}(Ce_{0.43}Nd_{0.19}La_{0.17}Ca_{0.11}Pr_{0.05}Y_{0.01})_{\Sigma 0.96}(Al_{0.90}Fe_{0.10})_{\Sigma 1.00}Al_{1.00}(Mg_{0.55}Fe_{0.43}Ti_{0\cdot 02})_{\Sigma 1.00}[Si_{3.04}O_{11}](OH,O)_2$.

Sample 14 (Varlamov et al., 2010; Maiorova et al., 2017) is from ores of the Tykotlovskoe gold–sulfide ore occurrence located in the northern part of the Subpolar Urals (Narodnaya Mt, Lemvinskii Allochthone). The zone of interbedding of gray and light gray rhyolite (felsite) with lava breccia and fluidal acid volcanic lavas contains the local areas schistosity and secondary silicification accompanied by the ore (gold–pyrite and gold–sulfide) mineralization. The ores are represented by veinlets of essentially pyrite or polymetallic composition (an association of sphalerite + galena + chalcopyrite ± pyrite). The most typical is the sphalerite–pyrite association with the galena matrix and minor chalcopyrite. Non-metal minerals are represented by quartz and minor carbonates (calcite and Zn–Mn carbonates). The grain size of accessory high-Ga minerals of the epidote and allanite groups is usually 20–50 μm, sometimes up to 100 μm by the long axis. They are characterized by the heterogeneous composition and contain three to five clearly distinctive chemical zones. The major sequence of zones from the center is the following: (1) minerals of the epidote group with the high and ultrahigh concentration of Ga (8–20 wt % Ga_2O_3) and almost free of REEs; (2) high-Ga ESMs with an intermediate and high concentrations of Ga (3–11 wt % Ga_2O_3) and REEs (3–20 wt % REE_2O_3; (3) allanite-(Ce) and epidote with the low Ga concentration (<2 wt % Ga_2O_3), intermediate and high REE concentration (4–19 wt % REE_2O_3); (4) epidote–allanite rims (often absent) without Ga and low or almost zero REE concentration (<6 wt % REE_2O_3). Sometimes the central zone (1) in grain sections is absent or includes small individual "spots" (Fig. 2c). We applied the method of Raman spectroscopy to the study of the high-Ga central zone, which is represented by a promising new mineral: Ga-dominated analogue of epidote, the first Ga silicate found in nature.

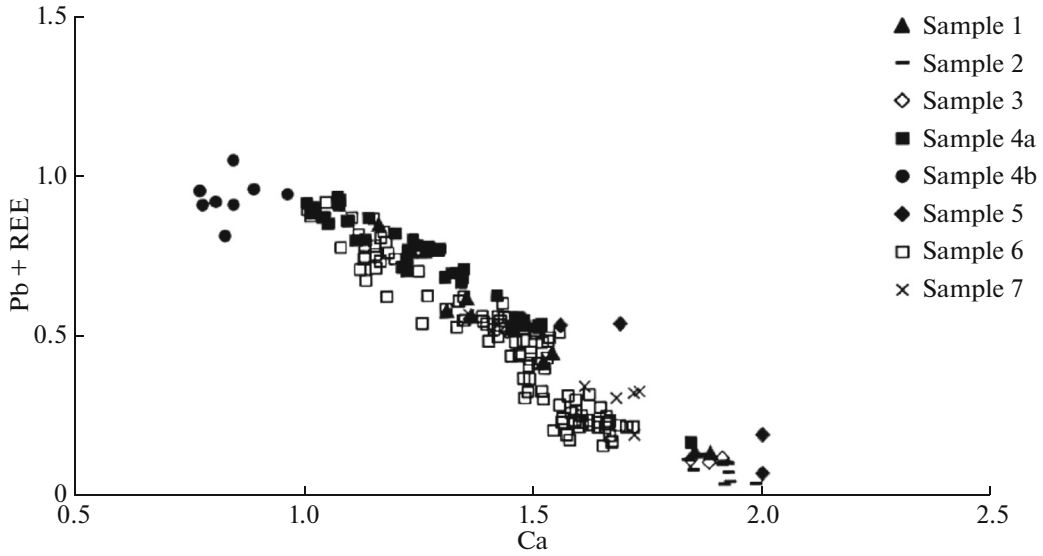

Fig. 3. Correlations between the total contents (pfu) of large cations (Pb, REEs) and Ca in epidote-supergroup minerals from the Pelagonian massif.

Sample 15 was collected from rocks of the dyke complex within the Kos'yuskoe ore field (Chetlasskii Kamen', Middle Timan) related to the Riphean Chetlasskii hypabyssal complex of alkaline picrite and carbonatite. It is represented by breccia composed of the fragments of alkaline picrite and host fenitized rocks cemented with albite, and abundant acicular apatite, single zoned clinopyroxene of the aegirine–augite series, with rims of amphibole, sulfides (chalcopyrite and pyrite), magnetite, and titanite. The fragments have essentially albite cores (often with quartz and calcite) and pyroxene–amphibole rims composed of an aggregate of laminar aegirine–augite, alkaline amphiboles, calcite, apatite, titanite (with 3.5 wt % Nb_2O_5), and single chrome spinellide relics. The ESMs studied in this association (Varlamov et al., 2017b) are represented by zoned individuals with a size up to 0.3 mm. They contain the central zones significantly enriched in chromium (up to 13 wt % Cr_2O_3) and REEs (up to 24–26 wt % REE_2O_3) at an anomalously low Al content (Fig. 2d).

RESULTS OF THE STUDY AND DISCUSSION

The typical chemical compositions of the ESMs from the studied samples are reported in Tables 1 and 2; their empirical and idealized formulae are presented in Table 3. The formula coefficients and distribution of the components over the sites of crystal structure were determined according to the rules accepted for the epidote supergroup (Armbruster et al., 2006). As follows from these data, the compositional series corresponds to nine potential mineral species. Unfortunately, due to small sizes of monomineral segregations, it was impossible to determine the valence state of iron and manganese in these minerals; thus, there is uncertainty in attribution of REE-bearing ESMs to a certain group (allanite or askagenite). Due to the high activity of oxygen in the processes of the formation of ore bodies in the Nežilov area (Chukanov et al., 2015, 2016), we may assume that most of Fe and Mn in the ESMs from these objects occur in the trivalent state.

The correlation analysis of the ESMs from the Nežilov area supports the previous conclusion (Armbruster et al., 2006) on the practically complete ordering of large cations (Pb and REEs) in the *A*2 site: there is the correlation between Ca and Pb + REE with $R = -0.95$. A slight dispersal of points on the graph of this correlation (Fig. 3) mostly results from incorporation of low contents of Mn^{2+} into the *A*1 site. Firstly, this is related to the compositions with the Ca concentration of <1 pfu (Sample 4). At the same time, the major cations occupying the *A*2 site (Ca, Pb, and REEs) demonstrate three clear trends on the ternary diagram (Fig. 4) that allows us to suggest three types of mineral-forming media. The first trend including most of the experimental points plotting near the (Ca-1)–Pb line is controlled by crystallization under the conditions of relatively low REE activity and variable Pb activity. The second and third trends (points on the Pb–ΣREE line and in the lower part of the ternary diagram) relate to the ESMs crystallized under the high REE activity, but under the conditions of the low and high Ca activity, respectively.

As is evident from the diagram (Fig. 5), the total compositions of the *A*1 and *A*3 sites accumulating Fe and Mn in samples from the Nežilov area vary in relatively narrow limits. Interestingly, the content of wittingly divalent octahedral cations (Cu^{2+}, Zn^{2+}, and

Table 1. Representative chemical compositions of epidote-supergroup minerals from the Pelagonian massif

Analysis no.	1	2	3	4	5	6	7	8
sample no.	1	4	1	1	1	6	7	4
component	Concentration, wt %							
CaO	14.13	11.86	13.75	9.70	12.70	12.84	13.52	6.82
PbO	7.03	26.34	5.61	29.90	8.94	7.31	10.36	15.63
CuO	1.81	B.d.l.	1.57	B.d.l.	1.93	0.77	B.d.l.	B.d.l.
ZnO	3.14	The same	1.71	0.49	3.28	3.90	3.46	0.87
MgO	B.d.l.	″	1.23	0.73	B.d.l.	0.32	0.64	0.43
Mn_2O_3	10.82	8.61	9.44	7.69	4.67	6.93	1.59	13.67
Fe_2O_3	5.76	8.75	6.48	11.23	9.35	7.15	10.61	8.32
La_2O_3	4.63	B.d.l.	7.73	B.d.l.	3.25	5.11	1.65	4.87
Ce_2O_3	1.23	The same	0.50	The same	3.91	3.38	3.88	4.49
Pr_2O_3	1.34	″	0.90	″	0.63	1.13	1.14	1.39
Nd_2O_3	3.63	″	3.36	″	2.72	2.18	2.25	2.40
Sm_2O_3	B.d.l.	″	B.d.l.	″	0.96	0.06	B.d.l.	B.d.l.
Eu_2O_3	The same	″	The same	″	0.48	B.d.l.	The same	The same
Gd_2O_3	″	″	0.19	″	B.d.l.	0.13	″	″
Tb_2O_3	″	″	0.11	″	The same	B.d.l.	″	″
Dy_2O_3	″	″	0.53	″	″	The same	″	″
Yb_2O_3	″	″	0.10	″	0.33	″	″	″
Al_2O_3	14.17	14.04	13.02	10.86	15.48	13.72	17.27	10.34
SiO_2	31.79	28.90	32.48	28.06	30.86	30.66	31.66	28.89
Total	99.49	99.97	98.71	98.66	99.49	95.59*	98.03	98.12
Formula coefficients calculated on 8 cations								
Ca	1.48	1.30	1.45	1.16	1.36	1.35	1.36	0.77
Pb	0.17	0.73	0.14	0.85	0.23	0.19	0.26	0.45
Cu	0.13	0	0.11	0	0.14	0.06	0	0
Zn	0.21	0	0.12	0.04	0.23	0.28	0.24	0.07
Mg	0	0	0.17	0.11	0	0.05	0.09	0.07
Mn	0.76	0.67	0.68	0.62	0.33	0.52	0.11	1.10
Fe	0.40	0.67	0.45	0.89	0.66	0.53	0.75	0.66
La	0.16	0	0.27	0	0.11	0.18	0.06	0.19
Ce	0.04	0	0	0	0.14	0.12	0.13	0.18
Pr	0.04	0	0	0	0.02	0.04	0.04	0.05
Nd	0.12	0	0.11	0	0.09	0.08	0.08	0.09
Sm	0	0	0	0	0.03	0	0	0
Eu	0	0	0	0	0.02	0	0	0
Gd	0	0	0	0	0	0	0	0
Tb	0	0	0	0	0	0	0	0
Dy	0	0	0	0	0	0	0	0
Yb	0	0	0	0	0.01	0	0	0
Al	1.54	1.69	1.43	1.35	1.71	1.59	1.91	1.29
Si	2.94	2.95	3.05	2.97	2.91	3.01	2.97	3.07

* The low total is explained by the small size of the analyzed homogeneous part of the grain.

Table 2. Representative chemical compositions of epidote-supergroup minerals from the Urals and Eifel

Analysis no.	9	10	11	12	13	14	15	16	17
sample no.	15	15	14	14	8	8	9	11	10
component	Concentration, wt %								
Na_2O	B.d.l.	B.d.l.	B.d.l.	B.d.l.	B.d.l.	B.d.l.	B.d.l.	B.d.l.	B.d.l.
CaO	9.63	9.38	21.51	20.91	6.07	5.83	10.65	8.02	6.74
PbO	0.22	B.d.l.	B.d.l.	B.d.l.	B.d.l.	B.d.l.	B.d.l.	B.d.l.	B.d.l.
ZnO	B.d.l.	The same	0.85	0.45	The same	The same	The same	The same	The same
MgO	0.93	1.01	0.07	B.d.l.	0.96	1.22	1.47	1.12	0.89
MnO	0.48	0.63	0.28	0.43	13.19	13.62	2.39	3.46	9.98
FeO	B.d.l.	B.d.l.	B.d.l.	B.d.l.	B.d.l.	B.d.l.	B.d.l.	B.d.l.	4.04
Fe_2O_3	17.44	16.65	4.15	4.43	7.47	7.79	15.92	20.03	7.39
Cr_2O_3	10.73	12.74	B.d.l.	B.d.l.	B.d.l.	B.d.l.	B.d.l.	B.d.l.	B.d.l.
La_2O_3	10.44	10.41	0.09	0.16	5.39	6.75	10.73	11.58	13.35
Ce_2O_3	11.58	11.38	0.38	0.66	8.04	6.98	10.83	11.28	10.58
Pr_2O_3	0.77	0.09	0.24	0.34	1.77	2.05	B.d.l.	0.63	0.42
Nd_2O_3	1.62	1.80	0.13	0.55	6.85	7.20	1.10	1.21	0.49
Sm_2O_3	0.20	B.d.l.	0.01	B.d.l.	B.d.l.	0.66	B.d.l.	B.d.l.	0.34
Eu_2O_3	0.25	The same	0.16	0.06	The same	B.d.l.	The same	The same	0.18
Gd_2O_3	0.52	″	0.16	B.d.l.	″	0.66	″	″	0.20
Dy_2O_3	0.21	″	B.d.l.	The same	″	B.d.l.	″	″	B.d.l.
Ho_2O_3	B.d.l.	″	The same	″	0.69	B.d.l.	″	″	The same
Y_2O_3	The same	″	″	″	B.d.l.	B.d.l.	″	″	″
Al_2O_3	2.96	2.87	19.20	17.44	14.76	15.22	12.81	10.31	11.47
Ga_2O_3	B.d.l.	B.d.l.	14.98	17.20	B.d.l.	B.d.l.	B.d.l.	B.d.l.	B.d.l.
SiO_2	27.92	28.11	36.05	35.42	34.23	31.42	31.19	29.99	29.80
TiO_2	3.04	3.08	0.09	B.d.l.	0.31	B.d.l.	0.99	B.d.l.	1.32
ThO_2	B.d.l.	B.d.l.	B.d.l.	The same	B.d.l.	The same	1.47	0.96	0.43
UO_2	The same	The same	The same	″	The same	″	B.d.l.	B.d.l.	0.10
Total	98.94	98.15	98.36	98.05	99.73	99.40	99.55	98.59	99.22
Formula coefficients calculated on 8 cations									
Na	0	0	0	0	0	0	0	0	0
Ca	1.08	1.04	1.92	1.90	0.64	0.60	1.10	0.86	0.72
Pb	0	0	0	0	0	0	0	0	0
Zn	0	0	0.05	0.03	0	0	0	0	0
Mg	0.14	0.16	0.01	0	0.14	0.17	0.21	0.17	0.13
Mn	0.05	0.06	0.02	0.03	1.10	1.10	0.19	0.29	0.85
Fe	1.38	1.30	0.26	0.28	0.56	0.56	1.15	1.51	0.90
Cr	0.89	1.04	0	0	0	0	0	0	0
La	0.40	0.40	0	0	0.20	0.24	0.38	0.43	0.49
Ce	0.43	0.43	0.01	0.02	0.29	0.24	0.38	0.41	0.39
Pr	0.03	0	0.01	0.01	0.06	0.07	0	0.02	0.02
Nd	0.06	0.07	0	0.02	0.24	0.25	0.04	0.04	0.02
Sm	0.01	0	0	0	0	0.02	0	0	0.01

Table 2. (Contd.)

Analysis no.	9	10	11	12	13	14	15	16	17
sample no.	15	15	14	14	8	8	9	11	10
component	Formula coefficients calculated on 8 cations								
Eu	0.01	0	0	0	0	0	0	0	0.01
Gd	0.02	0	0	0	0	0.02	0	0	0.01
Dy	0.01	0	0	0	0	0	0	0	0
Ho	0	0	0	0	0.02	0	0	0	0
Y	0	0	0	0	0	0	0	0	0
Al	0.36	0.35	1.89	1.75	1.72	1.72	1.45	1.22	1.36
Ga	0	0	0.80	0.94	0	0	0	0	0
Si	2.94	2.91	3.01	3.01	3.00	3.01	3.00	3.01	2.98
Ti	0.24	0.24	0.01	0	0.02	0	0.07	0	0.10
Th	0	0	0	0	0	0	0.03	0.02	0.01

Mg^{2+}) is rather high (up to 0.45 pfu) (Fig. 6). According to the data available (Armbruster et al., 2006), the divalent *M* cations show a strong tendency towards accumulation in the *M*3 site. Judging from the positive correlation ($R = 0.91$) between the total concentration of these elements and total REEs (Fig. 7), we may assume heterovalent isomorphism via the scheme: $^{A2}Ca^{2+} + {}^{M3}(Fe,Mn)^{3+} = {}^{A2}REE^{3+} + {}^{M3}(Zn,Cu,Mg)^{2+}$. Such correlation provides additional evidence for the predominant trivalent state of iron and manganese in the ESMs from the Nežilov area.

Zones with the highest Cr content in Sample 15 are the first example of the Cr-dominant ESM. Previously, high-Cr ESMs were found in Outokumpu, Finland (Treloar, 1987; Treloar and Charnley, 1987), New Zealand Southern Alps (Grapes, 1981), and Tanzania (Eppler, 1984); however, these finds are represented by the minerals with a low REE content. In the min-

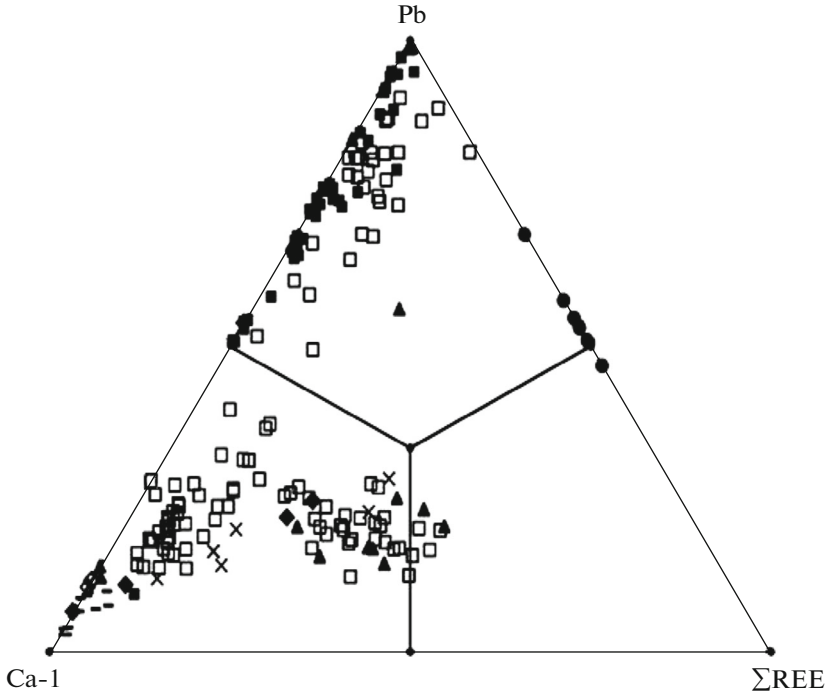

Fig. 4. Relationship between elements in the *A*2 site (Ca, Pb, and ΣREE, pfu) in epidote-supergroup minerals from the Pelagonian massif, in assumption that the *A*1 site contains Ca only. See Fig. 3 for the legend.

Table 3. Typical empirical and idealized formulae of studied epidote-supergroup minerals

Sample no.	Mineral	Empirical formula Idealized formula
1	Piemontite	$Ca_{1.00}(Ca_{0.48}Pb_{0.17}La_{0.16}Nd_{0.12}Ce_{0.04}Pr_{0.04})_{\Sigma 1.01}(Al_{0.48}Fe_{0.40}Mn_{0.12})_{\Sigma 1.00}Al_{1.00} \cdot (Mn_{0.64}Zn_{0.21}Cu_{0.13})_{\Sigma 0.98}[(Si_{2.94}Al_{0.06})_{3.00}O_{11}](OH,O)_2$ **$CaCaAlAlMn^{3+}(Si_3O_{12})(OH)$**
4	Piemontite-(Pb)*	$Ca_{1.00}(Pb_{0.73}Ca_{0.30})_{\Sigma 1.03}(Al_{0.64}Fe_{0.36})_{\Sigma 1.00}Al_{1.00}(Mn_{0.67}Fe_{0.31})_{\Sigma 0.98} \cdot [(Si_{295}Al_{0.05})_{\Sigma 3.00}O_{11}](OH,O)_2$ **$CaPbAlAlMn^{3+}(Si_3O_{12})(OH)$**
1	"Ferripiemontite"	$(Ca_{0.92}Mn_{0.08})_{\Sigma 1.00}(Ca_{0.53}La_{0.27}Pb_{0.14}Nd_{0.11})_{\Sigma 1.05}(Fe_{0.45}Al_{0.43})_{\Sigma 0.88}Al_{1.00}(Mn_{0.60} \cdot Mg_{0.17}Zn_{0.12}Cu_{0.11})_{\Sigma 1.00}[Si_{3.05}O_{11}](OH,O)_2$ **$CaCaFe^{3+}AlMn^{3+}(Si_3O_{12})(OH)$**
1	"Ferripiemontite-(Pb)"	$Ca_{1.00}(Pb_{0.85}Ca_{0.16})_{\Sigma 1.01}(Fe_{0.68}Al_{0.32})_{\Sigma 1.00}Al_{1.00}(Mn_{0.62}Fe_{0.21}Mg_{0.11}Zn_{0.04})_{\Sigma 0.98} \cdot [(Si_{2.97}Al_{0.03})_{\Sigma 3.00}O_{11}](OH,O)_2$ **$CaPbFe^{3+}AlMn^{3+}(Si_3O_{12})(OH)$**
1	Mineral of the askagenite group or Ca analog (in the *A*1 site) of androsite-(Ce)	$Ca_{1.00}[(Ce_{0.14}La_{0.11}Nd_{0.09}Sm_{0.03}Pr_{0.02}Eu_{0.02}Yb_{0.01})_{\Sigma 0.42}Ca_{0.36}Pb_{0.23}]_{\Sigma 1.01} \cdot (Al_{0.62}Fe_{0.38})_{\Sigma 1.00}Al_{1.00}(Mn_{0.33}Fe_{0.28}Zn_{0.23}Cu_{0.14})_{\Sigma 0.98}(Si_{2.91}Al_{0.09})_{\Sigma 3.00}O_{11}](O,OH)_2$ **$CaCeAlAlMn^{3+}(Si_3O_{12})O$ and $CaCeAlAlMn^{2+}(Si_3O_{12})(OH)$**
6	Mineral of the askagenite group or Ca analog (in the *A*1 site) of androsite-(La)	$(Ca_{0.97}Mn_{0.03})_{\Sigma 1.00}[(La_{0.18}Ce_{0.12}Nd_{0.\ 08}Pr_{0.04})_{\Sigma 0.42}Ca_{0.38}Pb_{0.19}]_{\Sigma 0.99}(Al_{0.59} \cdot Fe_{0.41})_{\Sigma 1.00}Al_{1.00}(Mi_{0.49}Zn_{0.28}Fe_{0.12}Cu_{0.06}Mg_{0.05})_{\Sigma 1.00}[S_{i3.01}O_{11}](O,OH)_2$ **$CaLaAlAlMn^{3+}(Si_3O_{12})O$ and $CaLaAlAlMn^{2+}(Si_3O_{12})(OH)$**
7	Epidote	$(Ca_{0.93}Mn_{0.07})_{\Sigma 1.00}(Ca_{0.43}Pb_{0.26}Ce_{0.13}Nd_{0.08}La_{0.06}Pr_{0.04})_{\Sigma 1.00}(Al_{0.88}Fe_{0.12})_{\Sigma 1.00} \cdot Al_{1.00}(Fe_{0.63}Zn_{0.24}Mg_{0.09}Mn_{0.04})_{\Sigma 1.00}(Si_{2.97}Al_{0.03})_{\Sigma 3.00}O_{11}](OH,O)_2$ **$CaCaAlAlFe(Si_3O_{12})(OH)$**
4	Mineral of the askagenite group or Mn^{2+} analog of "ferridissakisite"	$(Ca_{0.77}Mn_{0.19})_{\Sigma 0.96}[(La_{0.19}Ce_{0.18}Nd_{0.09}Pr_{0.05})_{\Sigma 0.51}Pb_{0.45}]_{\Sigma 0.96}(Fe_{0.66}Al_{0.29} \cdot Mg_{0.05})_{\Sigma 1.00}Al_{1.00}(Mn_{0.91}Zn_{0.07}Mg_{0.02})_{\Sigma 1.00}[Si_{3.07}O_{11}](O,OH)_2$ **$CaLaFe^{3+}AlMn^{3+}(Si_3O_{12})O$ and $CaLaFe^{3+}AlMn^{2+}(Si_3O_{12})(OH)$**
15	Mineral of the askagenite group or Cr analog (in the *M*2 site) of ferriallanite-(Ce)**	$Ca_{1.00}(Ce_{0.43}La_{0.40}Ca_{0.08}Nd_{0.06}Pr_{0.03})_{\Sigma 1.00}(Fe_{0.81}Cr_{0.19})_{\Sigma 1.00}(Cr_{0.70}Al_{0.30})_{\Sigma 1.00} \cdot (Fe_{0.57}Ti_{0.24}Mg_{0.14}Mn_{0.05})_{\Sigma 1.00}[(Si_{2.94}Al_{0.06})_{\Sigma 3.00}O_{11}](O,OH)_2$ **$CaCeFeCrFe^{3+}(Si_3O_{12})O$ and $CaCeFeCrFe^{2+}(Si_3O_{12})(OH)$**
15	Mineral of the askagenite group or Cr analog (in the *M*2 site) of ferriallanite-(Ce)	$(Ca_{0.94}Mn_{0.06})_{\Sigma 1.00}(Ce_{0.43}La_{0.40}Ca_{0.10}Nd_{0.07})_{\Sigma 1.00}(_{Fe0.70}Cr_{0.30})_{\Sigma 1.00}(Cr_{0.74} \cdot Al_{0.26})_{\Sigma 1.00}(Fe_{0.60}Ti_{0.24}Mg_{0.16})_{\Sigma 1.00}[(Si_{2.91}Al_{0.09})_{\Sigma 3.00}O_{11}](O,OH)_2$ **$CaCeFe^{3+}CrFe^{3+}(Si_3O_{12})O$ and $CaCeFe^{3+}CrFe^{2+}(Si_3O_{12})(OH)$**
14	Ga analog (in the *M*3 site) of epidote**	$(Ca_{0.98}Mn_{0.02})_{\Sigma 1.00}(Ca_{0.94}Ce_{0.01}Pr_{0.01})_{\Sigma 0.96}(Al_{0.89}Fe_{0.11})_{\Sigma 1.00}Al_{1.00}(Ga_{0.80}Fe_{0.15} \cdot Zn_{0.05}Ti_{0.01}Mg_{0.01})_{\Sigma 1.02}[Si_{3.01}O_{11}](OH,O)_2$ **$CaCaAlAlGa(Si_3O_{12})(OH)$**
14	Ga analog (in the *M*3 site) of epidote	$(Ca_{0.97}Mn_{0.03})_{\Sigma 1.00}(Ca_{0.93}Ce_{0.02}Nd_{0.02}Pr_{0.01})_{\Sigma 0.98}(Al_{0.75}Fe_{0.25})_{\Sigma 1.00}Al_{1.00}(Ga_{0.94} \cdot Fe_{0.03}Zn_{0.03})_{\Sigma 1.00}[Si_{3.01}O_{11}](OH,O)_2$ **$CaCaAlAlGa(Si_3O_{12})(OH)$**
8	Mineral of the askagenite group or Mn^{2+} analog (in the *M*3 site) of uedaite-(Ce)	$(Mn_{0.54}Ca_{0.46})_{\Sigma 1.00}(Ce_{0.29}Nd_{0.24}La_{0.20}Ca_{0.18}Pr_{0.06}Ho_{0.02})_{\Sigma 0.99}(Al_{0.72}Fe_{0.28})_{\Sigma 1.00} \cdot Al_{1.00}(Mn_{0.56}Fe_{0.28}Mg_{0.14}Ti_{0.02})_{\Sigma 1.00}[Si_{3.00}O_{11}](O,OH)_2$ **$Mn^{2+}CeAlAlMn^{3+}(Si_3O_{12})O$** and **$Mn^{2+}CeAlAlMn^{2+}(Si_3O_{12})(OH)$**
8	Mineral of the askagenite group or Mn^{2+} analog (in the *M*3 site) of uedaite-(Nd)	$(Mn_{0.55}Ca_{0.45})_{\Sigma 1.00}(Nd_{0.25}Ce_{0.24}La_{0.24}Ca_{0.15}Pr_{0.07}Sm_{0.02}Gd_{0.02})_{\Sigma 0.99}(Al_{0.72} \cdot Fe_{0.28})_{\Sigma 1.00}Al_{1.00}(Mn_{0.55}Fe_{0.28}Mg_{0.17})_{\Sigma 1.00}[Si_{3.01}O_{11}](O,OH)$ **$Mn^{2+}NdAlAlMn^{3+}(Si_3O_{12})O$ and $Mn^{2+}NdAlAlMn^{2+}(Si_3O_{12})(OH)$**

Table 3. (Contd.)

Sample no.	Mineral	Empirical formula Idealized formula
9	Ferriallanite (Ce/La)	$(Ca_{0.93}Mn_{0.07})_{\Sigma 1.00}(Ce_{0.38}La_{0.38}Ca_{0.17}Nd_{0.04}Th_{0.03})_{\Sigma 1.00}(Fe_{0.55}Al_{0.45})_{\Sigma 1.00} \cdot Al_{1.00}(Fe_{0.60}Mg_{0.21}Mn_{0.12}Ti_{0.07})_{\Sigma 1.00}[Si_{3.00}O_{11}](OH,O)_2$ **$CaCeFe^{3+}AlFe^{2+}(Si_3O_{12})OH$ and $CaLaFe^{3+}AlFe^{2+}(Si_3O_{12})OH$**
11	Ferriallanite (La)	$(Ca_{0.81}Mn_{0.19})_{\Sigma 1.00}(La_{0.43}Ce_{0.41}Ca_{0.05}Nd_{0.04}Pr_{0.02}Th_{0.02})_{\Sigma 0.97}(Fe_{0.78}Al_{0.22})_{\Sigma 1.00} \cdot Al_{1.00}(Fe_{0.73}Mg_{0.17}Mn_{0.10})_{\Sigma 1.00}[Si_{3.01}O_{11}](O,OH)_2$ **$CaLaFe^{3+}AlFe^{2+}(Si_3O_{12})OH$**
10	Ferriakasakaite-(La);	$(Ca_{0.68}Mn^{2+}_{0.32})_{\Sigma 1.00}(La_{0.49}Ce_{0.39}Ca_{0.04}Pr_{0.02}Nd_{0.02}Sm_{0.01}Eu_{0.01}Gd_{0.01} \cdot Th_{0.01})_{\Sigma 1.00}(Fe^{3+}_{0.52}Al_{0.34}Ti^{4+}_{0.10}Fe^{2+}_{0.04})_{\Sigma 1.00}Al_{1.00}(Mn^{2+}_{0.53}Fe^{2+}_{0.34}Mg_{0.13})_{\Sigma 1.00} \cdot [(Si_{2.98}Al_{0.02})_{\Sigma 3.00}O_{11}](OH,O)_2$ **$CaLaFe^{3+}AlMn^{2+}(Si_3O_{12})OH$**

* The average composition, data from (Chukanov et al., 2012).
** The average composition. Other formulae correspond to the local compositions. The formulae of assumed end members corresponding by the promising new mineral species are given by bold.

eral from this study, Cr mostly substitutes for Al (with a correlation coefficient of –0.92) and, to a lesser extent, iron.

Unfortunately, Raman spectra of the studied samples of ESMs do not allow us to estimate the content of OH groups in them due to the strong luminescence and noise in the area of wavenumbers above 2000 cm^{-1}. However, even comparison of the Raman spectra in the range of 100–1200 cm^{-1} (Figs. 8 and 9) allows us to make some important conclusions.

It is known that the position of the band within the range of 1020–1200 cm^{-1} related to stretching vibrations of the Si–O–Si bridge depends on the value of the Si–O–Si angle: the higher this angle, the higher the frequency of corresponding vibrations (Chukanov, 2014). As is evident from Figs. 8 and 9, the wavenum-

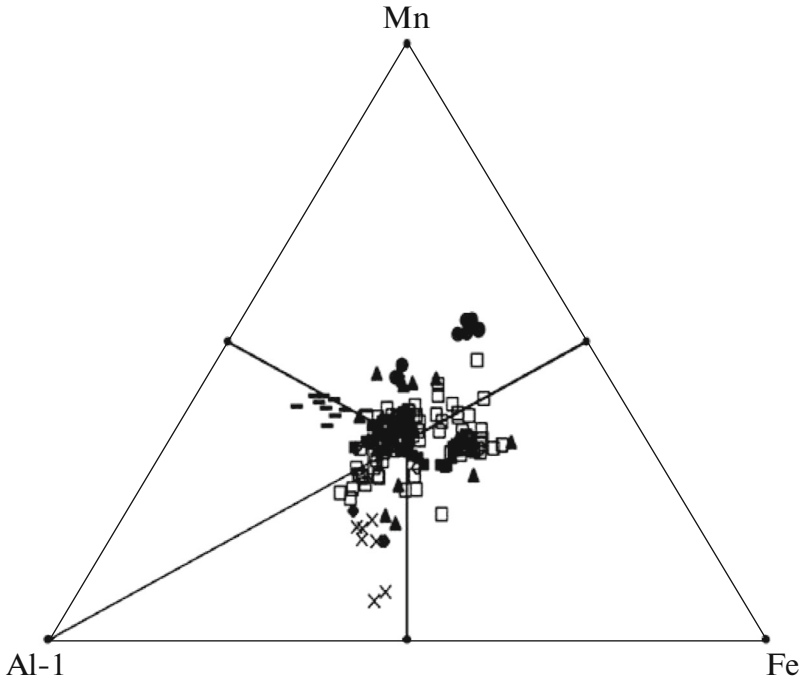

Fig. 5. Relationship between major elements (Al, Mn, and Fe, pfu) in the *M*1 and *M*3 sites of epidote-supergroup minerals from the Pelagonian massif, in assumption that the *M*2 site contains Al only. See Fig. 3 for the legend.

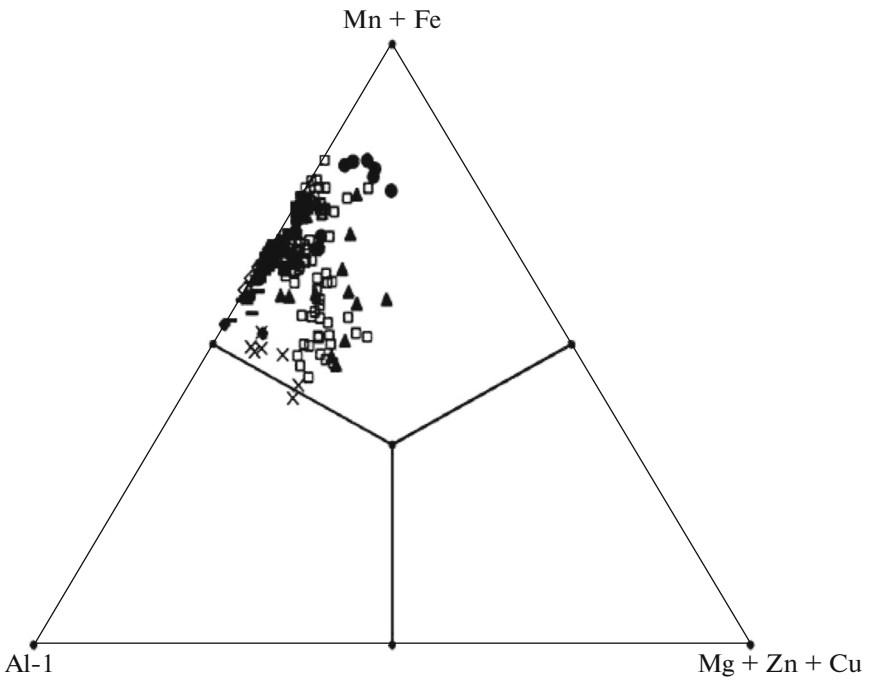

Fig. 6. Relationship between Al, Mn + Fe and Mg + Zn + Cu (pfu) in the *M*1 and *M*3 sites of epidote-supergroup minerals from the Pelagonian massif, under assumption that the *M*2 site contains Al only. See Fig. 3 for the legend.

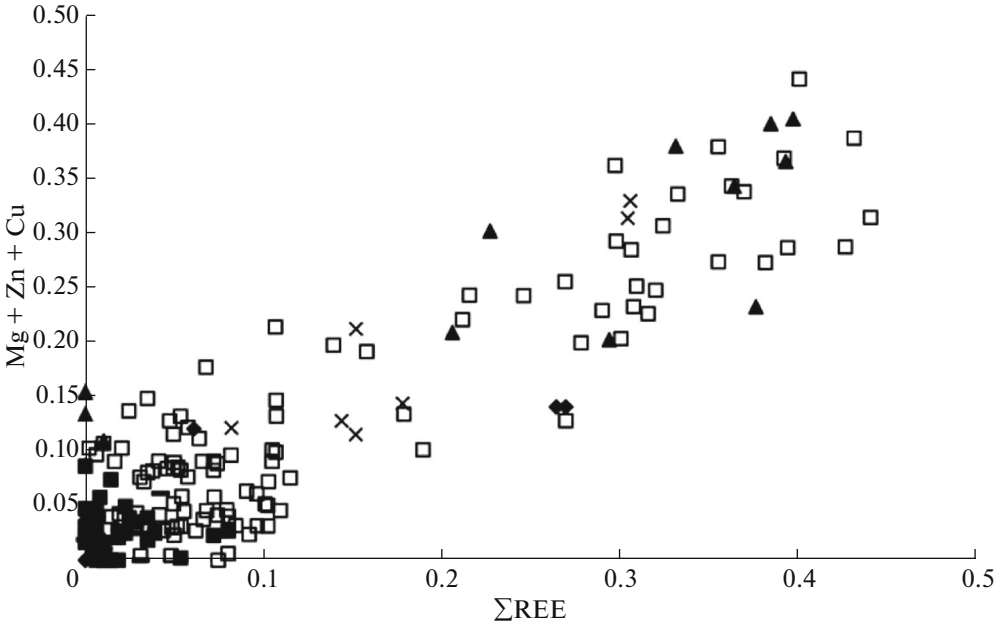

Fig. 7. Correlation between REEs and Mg + Zn + Cu (pfu) in epidote-supergroup minerals from the Pelagonian massif (Macedonia). See Fig. 3 for the legend.

ber of this band for REE-bearing ESMs ranges within 1024–1056 cm^{-1}, whereas the wavenumbers for the band in REE-free samples including piemontite-(Pb) with a large cation Pb^{2+} vary within 1074–1078 cm^{-1}. From this, we can conclude that the angle Si–O–Si in the $Si_2O_7^{6-}$ group depends on the force characteristics rather than on size of a cation in the *A*2 site. This conclusion agrees with the data of X-ray structural analysis for ESMs. For example, the Si–O–Si angle in the ferriallanite-(La) structure is 143.61° (Kolitsch et al., 2012), while this angle for epidote is 154.59 (Gatta et al., 2010).

The comparison of Raman spectra of piemontite and piemontite-(Pb) shows that the latter has wider

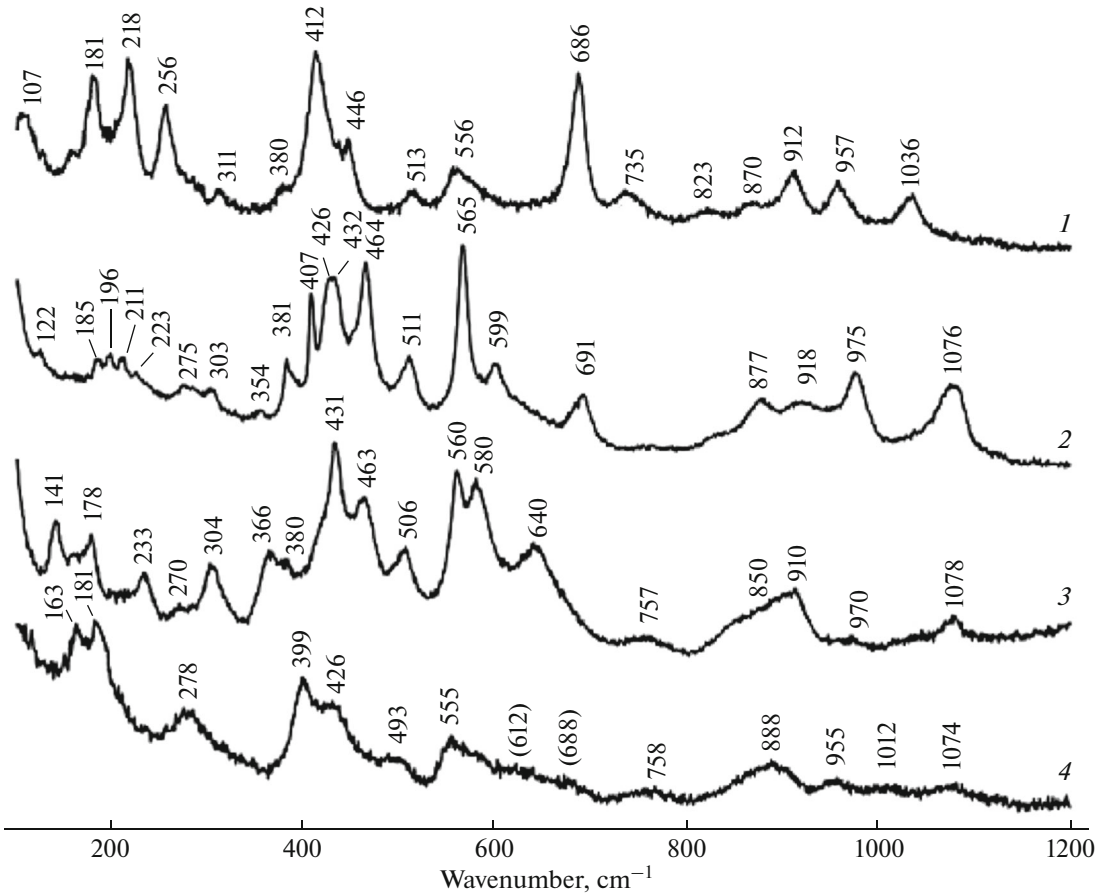

Fig. 8. Raman spectra of the Cr-rich allanite-group mineral from Sample 15 (*1*), Ga-rich epidote-supergroup mineral from Sample 14 (*2*), piemontite from Sample 12 (*3*), and the holotype of piemontite-(Pb) from Sample 4 (*4*).

bands, and most of them are shifted to the low-frequency area, which may be explained by involvement of a heavy cation Pb^{2+} to vibrations of this type. The band resolution of bands in Raman spectra of the samples from Eifel and Mochalin Log results from the presence of low contents thorium in their compositions, since radioactive decay of this element leads to accumulation of structural defects in this mineral. At the early stages of ESM metamictization, the presence of structural defects has an insignificant impact on X-ray diffraction patterns of these minerals, which, for example, is evident from the data of X-ray structural analysis of ESMs from Eifel (Kolitsch et al., 2012; Chukanov et al., 2018). Thus, Raman spectra of ESMs, as well as their IR spectra (Chukanov, 2014), are sensitive to radiation damage, which can be used as a method of monitoring the radiation resistance of similar materials when they are used to immobilize actinides.

The spectrum range of 300–600 cm^{-1} shows an appearance of the *M*–O stretching vibrations, where *M* is the octahedrally coordinated cation. Due to the collective character of these vibrations, and their resonance with bending vibrations of silicate anions, it is impossible to understand the relationship between the spectral bands in this range and certain *M* cations.

CONCLUSIONS

The data obtained in this study significantly expands our knowledge on the chemical composition of ESMs. In particular, Ga-bearing minerals of this supergroup including the Ga-dominant member of the epidote group (the first Ga silicate found in nature), Cr-dominant member of the allanite group, and unusual Al-deficient minerals of the epidote group with the high concentration of chalcophile elements (Pb, Zn, and Cu) have been described for the first time. The correlations obtained allow us to make reasonable assumptions about the distribution of cations over various sites in the crystal structures of the studied minerals. Based on these data, we may suggest nine promising new mineral species in the epidote supergroup with the following simplified formulae:

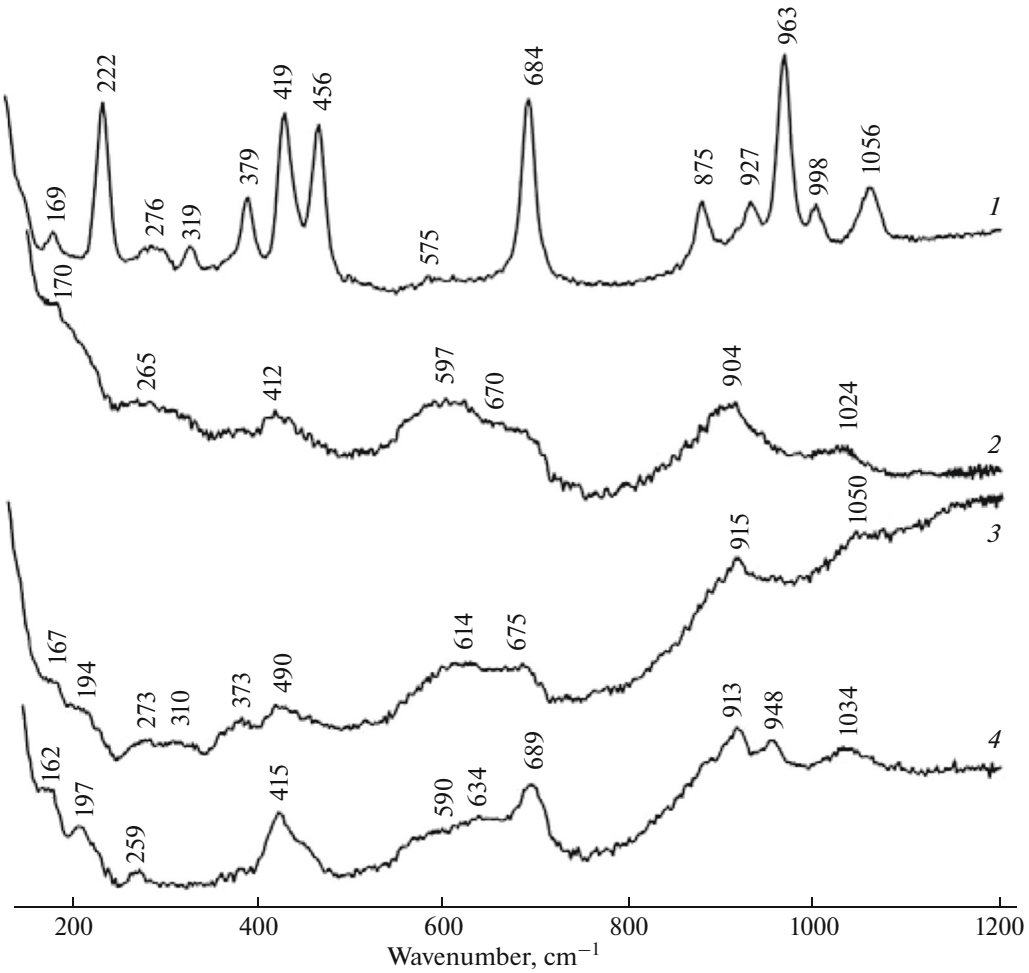

Fig. 9. Raman spectra of dissakisite-(Ce) from Sample 13 (*1*), ferriallanite-(La) from Sample 11 (*2*), ferriallanite-(La/Ce) from Sample 9 (*3*), and ferriakasakaite-(La) from Sample 10 (*4*).

$$CaCaFe^{3+}AlMn^{3+}(Si_3O_{12})(OH),\ CaPbFe^{3+}AlMn^{3+}(Si_3O_{12})(OH),$$
$$CaCeAlAl(Mn^{2+},Mn^{3+})(Si_3O_{12})(OH,O),\ CaLaAlAl(Mn^{2+},Mn^{3+})(Si_3O_{12})(OH,O),$$
$$CaLaFe^{3+}Al(Mn^{2+},Mn^{3+})(Si_3O_{12})(OH,O),\ CaCeFe^{3+}Cr(Fe^{2+},Fe^{3+})(Si_3O_{12})(OH,O),$$
$$CaCaAlAlGa(Si_3O_{12})(OH),Mn^{2+}CeAlAl(Mn^{2+},Mn^{3+})(Si_3O_{12})(OH,O)$$
$$\text{and}\ Mn^{2+}NdAlAl(Mn^{2+},Mn^{3+})(Si_3O_{12})(OH,O).$$

In addition, the data obtained allow us to make the conclusion on the possibility of the application of Raman spectroscopy for estimation of the degree of defectiveness of ESMs containing impurities of radioactive elements at the early stages of their metamictization.

FUNDING

This study was supported by the Russian Foundation for Basic Research, project nos. 18-05-00051-a (study of the samples from the Nežilov area) and 18-29-12007_mk (study of other samples).

REFERENCES

Armbruster, T.H., Bonazzi, P., Akasaka, M., Bermanec, V., Chopin, C., Giere, R., Heuss-Assbichler, S., Liebscher, A., Menchetti, S., Pan, Y., and Pasero, M., Recommended nomenclature of epidote-group minerals, *Eur. J. Mineral.*, 2006, vol. 18, pp. 551–567.

Barić, L., Piemontit, gahnit und rutil aus dem Fundort der Blei und Zinkerze bei dem Dorfe Nezilovo in Mazedonien,

Glasnik Prirodnjackog Muzeja. Beograd. Ser. A, 1960, vol. 13, pp. 200–204.

Chukanov, N.V., *Infrared Spectra of Mineral Species: Extended Library*, Dordrecht–Heidelberg–New York–London: Springer-Verlag, 2014.

Chukanov, N.V., Aksenov, S.M., Jančev, S., Pekov, I.V., Göttlicher, J., Polekhovsky, Yu.S., Rusakov, V.S., Nelyubina, Yu.V., and Van, K.V., A new mineral species ferricoronadite, $Pb[Mn_6^{4+}(Fe^{3+},Mn^{3+})_2]O_{16}$: mineralogical characterization, crystal chemistry and physical properties, *Phys. Chem. Mineral.*, 2016, vol. 43, pp. 503–514.

Chukanov, N.V., Göttlicher, J., Möckel, S., Sofer, Z., and Belakovskiy, D.I., Åskagenite-(Nd), $Mn^{2+}NdAl_2Fe^{3+}(Si_2O_7)(SiO_4)O_2$, a new mineral of the epidote supergroup, *New data Mineral.*, 2010, vol. 45, pp. 17–22.

Chukanov, N.V., Jančev, S., and Pekov, I.V., The association of oxygen-bearing minerals of chalcophile elements in the orogenetic zone related to the "mixed series" complex near Nežilovo, Republic of Macedonia, *Macedon. J. Chem. Chem. Eng.*, 2015, vol. 34, no. 1, pp. 115–124.

Chukanov, N.V., Krivovichev, S.V., Pakhomova, A.S., Pekov, I.V., Schäfer, Ch., Vigasina, M.F., and Van, K.V., Laachite, $(Ca,Mn)_2Zr_2Nb_2TiFeO_{14}$, a new zirconolite-related mineral from the Eifel volcanic region, Germany, *Eur. J. Mineral.*, 2014, vol. 26, pp. 103–111.

Chukanov, N.V., Varlamov, D.A., Nestola, F., Belakovskiy, D.I., Göettlicher, J., Britvin, S.N., Lanza, A., and Jančev, S., Piemontite-(Pb), $CaPbAl_2Mn^{3+}[Si_2O_7][SiO_4]O(OH)$, a new mineral species of the epidote supergroup, *Neues Jahrb. Mineral.-Abh.*, 2012, vol. 189, no. 3, pp. 275–286.

Chukanov, N.V., Zubkova, N.V., Schäfer, C., Varlamov, D.A., Ermolaeva, V.N., Polekhovsky, Yu.S., Jancev, S., Pekov, I.V., and Pushcharovsky, D.Yu., New data on ferriakasakaite-(La) and related minerals extending the compositional field of the epidote supergroup, *Eur. J. Mineral.*, 2018, vol. 30, no. 2, pp. 323–332.

Eppler, W.F., *Praktische Gemmologie, 2nd ed*, Stuttgart: Ruhle-Diebener-Verlag, 1984.

Ermolaeva, V.N., Chukanov, N.V., Jančev, S., and Van, K.V., Endogenic oxide parageneses with chalcophile elements in the orogenic zone related to the "Mixed series" of the Pelagonian massif, republic of Macedonia, *New Data mineral.*, 2016, vol. 51, pp. 12–19.

Ermolaeva, V.N., Varlamov, D.A., Jančev, S., and Chukanov, N.V., Spinel-group and högbomite-supergroup minerals from a nonsulfide endogeneous Pb–Zn–Sb–As association in the Pelagonian massif, Macedonia, *Zap. Ross. Mineral. O-va*, 2018, vol. 147, no. 3, pp. 27–43.

Frechen, J., Vorgänge der Sanidinit-Bildung im Laacher Seegebiet, *Fortschr. Mineral.*, 1947, vol. 26, pp. 147–166.

Gatta, G.D., Meven, M., and Bromiley, G., Effects of temperature on the crystal structure of epidote: a neutron single-crystal diffraction study at 293 and 1070 K, *Phys. Chem. Mineral.*, 2010, vol. 37, pp. 475–485.

Grapes, R.H., Chromian epidote and zoisite in kyanite amphibolite, Southern Alps, New Zealand, *Am. Mineral.*, 1981, vol. 66, pp. 974–975.

Jančev, S., Chukanov, N.V., and Ermolaeva, V.N., Association of oxide minerals—concentrators of chalcophile elements (Pb, Zn, Sb) from the "Mixed series" near Nežilovo village, Macedonia, *Mat. Third Congress of Geologists of Republic of Macedonia, Struga*, 2016, vol. 2, pp. 401–404.

Kolitsch, U., Mills, S.J., Miyawaki, R., and Blass, G., Ferriallanite-(La), a new member of the epidote supergroup from the Eifel, Germany, *Eur. J. Mineral*, 2012, vol. 24, pp. 741–747.

Kuznetsov, E.A., Petrographic review of Mochalin Log, *Redkozzemel'nye mineraly Kyshtymskoi oblasti. Mater. Inst. Prikl. Mineral.* (Rare-Earth Minerals of thr Kyshtym Area Tr. Inst. Prikl. Mineral.), 1930, vol. 44, pp. 58–72.

Mayorova T.P., Varlamov D.A., and Soboleva, A.A., Mineralogy and geochemistry of Tykatlova gold-bearing occurrence with gallium mineralization (Sub-Polar Urals), *Osnovnye problem v uchenii ob endogennykh rudnykh mestorozhdeniyakh: novye gorizonty. Mat. Vseross. Konf. Posv. 120-letiyyu A.G. Betekhtina, Moskva, 2017* (The Main Issues in the Theory of Endogenous Ore Deposits: New Horizons. All-Russ. Conf. devoted to the 120th anniversary of A. G. Betekhtin), Moscow: IGEM RAS, 2017. P. 99–103.

Mills, S.J., Hatert, F., Nickel, E.H., and Ferraris, G., The standartization of mineral group hierarchies: application to recent nomenclature proposals, *Eur. J. Mineral*, 2009, vol. 21, pp. 1073–1080.

Moine, B., Fortune, J.P., Moreau, P., and Viguier, F., Comparative mineralogy, geochemistry, and conditions of formation of two metasomatic talc and chlorite deposits; Trimouns (Pyrenees, France) and Rabenwald (Eastern Alps, Austria), *Econ. Geol*, 1989, vol. 84, no. 5, pp. 1398–1416.

Ödman, O. H., Manganese mineralization in the Ultevis district, Jokkmokk, North Sweden. Part 2: Palache, C., *The minerals of Franklin and Sterling Hill Sussex County, New Jersey*, Washington: United States Government Printing Office, 1937.

Palache, Ch., A comparison of the ore deposits of Longban, Sweden, with those of Franklin, New Jersey, *Am. Mineral.*, 1929, vol. 14, no. 2, pp. 43–47.

Pekov, I.V., Alimova, A.N., Kononkova, N.N., and Kanonerov, A.A., To mineralogy of Mochalin Log in South Urals. I. Minerals of the bastnaesite family: history of studying and new data, *Ural. Geol. Zh.*, 2002, vol. 4, no. 28, pp. 127–144.

Piret, P., Deliens, M., and Pinet, M., La trimounsite-(Y), nouveau silicotitanate de terres rares de Trimouns, Ariège, France: $(TR)_2Ti_2SiO_9$, *Eur. J. Mineral.*, 1990, vol. 2, pp. 725–729.

Schmitt, A.K., Laacher See revisited: High-spatial-resolution zircon dating indicates rapid formation of a zoned magma chamber, *Geology*, 2006, vol. 34, pp. 597–600.

Schmitt, A.K., Wetzel, F., Cooper, K.M., Zou, H., and Worner, G., Magmatic longevity of Laacher See volcano

(Eifel, Germany) indicated by U-Th dating of intrusive carbonatites, *J. Petrol.*, 2010, vol. 51, pp. 1053–1085.

Svyazhin, N.V., Primary deposits of rare-earth and rare-metal minerals of Mochalin Log, Kyshtym district, Chelyabinsk Region, *Tr. Sverlovsk, Gorn. Inst.*, 1956, vol. 18, pp. 88–98.

Treloar, P.J. and Charnley, N.R., Chromian allanite from Outokumpu, Finland, *Can. Mineral.*, 1987, vol. 25, pp. 413–418.

Treloar, P.J., Chromian muscovites and epidotes from Outokumpu. Finland, *Mineral. Mag.*, 1987, vol. 51, pp. 593–599.

Varlamov, D.A. Ermolaeva, V.N. Jančev, C., and Chukanov, N.V., Oxides of the Pyrochlore Supergroup from a Nonsulfide Endogenic Assemblage of Pb–Zn–Sb–As Minerals in the Pelagonian Massif, Macedonia, *Geol. Ore Dep.*, 2018, vol. 60, no. 8, pp. 717–725.

Varlamov, D.A., Soboleva, A.A., and Mayorova, T.P., Galloepidote—new end-member in epidote group, *IMA 2010, 20th General Meeting of the International Mineralogical Association*, Budapest: 2010.

Varlamov, D.A., Udoratina, O.V., and Burakov, N.N., High-chromium ferriallanite—new mineral of epidote supergroup? *Mat. Yubilei. S'ezda Ross. Mineral. O-va 200 let RMO* (Proc. Jubilee Congress of Russian Mine O-va, 200 let RMO, St. Petersburg: Lema, 2017b, vol. 2, pp. 195–197.

Yudovich, Ya.E., Efanova, L.I., Shvetsova, I.V., Kozyreva, I.V., and Kotelnikova, E.A., *Zone of interformational contact in the kara of Lake Grubependity*, Syktyvkar: Geoprint, 1998.

Yudovjch, Ya.E., Kozyreva, I.V., Ketris, M.P., and Shvetsova, I.V., Geochemistry of rare earth elements in the zone of interformational contact on the Maldynyrd Ridge (Near-Polar Urals), *Geochem. Int.*, 2001, vol. 39, no. 1, pp. 1–12.

Translated by A. Bobrov